CMS Physics Analysis Summary

Contact: cms-pag-conveners-exotica@cern.ch 2016/08/05

Search for a high-mass resonance decaying into a dilepton final state in 13 fb^{-1} of pp collisions at $\sqrt{s} = 13$ TeV

The CMS Collaboration

Abstract

A search for new narrow resonances in dielectron and dimuon spectra is performed using data obtained from 2016 proton-proton collisions at 13 TeV. The integrated luminosity corresponds to 12.4 fb^{-1} and 13.0 fb^{-1} for the dielectron and dimuon samples, respectively. No significant deviations from the standard model expectation are observed. Upper bounds are set on the masses of hypothetical particles that arise in new-physics scenarios.

1 Introduction

The dilepton (ee or $\mu\mu$) final state signature is a key search channel for various new phenomena expected in theories that go beyond the standard model (SM). One of the most clean signatures would be the observation of a narrow resonance in the invariant mass spectrum of lepton pairs, predicted by many models at the TeV scale [1]. Examples include models described with extended gauge groups, featuring additional $U(1)$ symmetries such as the sequential standard model (SSM) [2] that includes a Z'_{SSM} boson with SM-like couplings and the grand unification theories (GUT) inspired models, based on E_6 gauge group, with a Z'_{ψ} boson [3, 4]. This search channel benefits from high signal selection efficiencies and relatively small, well-understood backgrounds.

Both the ATLAS and CMS collaborations have previously reported searches for a Z′ decaying to an electron pair or a muon pair [5, 6] using data collected in 2015 at $\sqrt{s} = 13\,\text{TeV}$ and corresponding to integrated luminosities of 3.2 fb^{-1} and 2.8 fb^{-1}, respectively. These results both compute limits at 95% confidence level combining the electronic and muonic channel and exclude Z'_{SSM} (Z'_{Ψ}) with a mass less than 3.15 (2.60) TeV for CMS and 3.36 (2.74) TeV for ATLAS.

This report presents the result of a new search for such a Z′ in the ee and $\mu^+\mu^-$ final states. The search is performed using pp collisions collected by the CMS experiment at the LHC operating at $\sqrt{s} = 13$ TeV in 2016, corresponding to integrated luminosities of $12.4\,\text{fb}^{-1}$ and $13.0\,\text{fb}^{-1}$ for the dielectron and dimuon analysis, respectively. The method is very similar to that of the previous CMS analysis performed at $\sqrt{s} = 13$ TeV in 2015 [6]. The results of the analysis are expressed in terms of the ratio of the cross section times branching fraction for a possible new narrow resonance to the same quantity for the Z boson. This approach reduces the impact of many known and unknown experimental and theoretical systematic uncertainties.

2 The CMS Detector

The central feature of the CMS detector is a superconducting solenoid providing an axial magnetic field of 3.8 T and enclosing an inner tracker, an electromagnetic calorimeter (ECAL), and a hadron calorimeter (HCAL). The inner tracker is composed of a silicon pixel detector and a silicon strip tracker, and measures charged-particle trajectories in the pseudorapidity range $|\eta| < 2.5$. The ECAL and HCAL, each composed of a barrel and two endcap sections, extend over the range $|\eta| < 3.0$. The finely segmented ECAL consists of nearly 76 000 lead tungstate crystals while the HCAL is constructed from alternating layers of brass and scintillator. Forward hadron calorimeters encompass $3.0 < |\eta| < 5.0$. The muon detection system, covering $|\eta| < 2.4$, consists of up to four layers of gas-ionization chambers installed outside the solenoid and sandwiched between the layers of the steel flux-return yoke. A more detailed description of the CMS detector, together with a definition of the coordinate system used and the relevant kinematic variables, can be found in Ref. [7].

The CMS experiment uses a two-level trigger system. The level-1 (L1) trigger [8], composed of custom hardware processors, selects events of interest using information from the calorimeters and muon detectors and reduces the readout rate from the 40 MHz bunch-crossing frequency to a maximum of 100 kHz. The high level trigger (HLT) [9] uses software algorithms accessing the full event information, including that from the inner tracker, to reduce the event rate to the 1 kHz that is recorded.

3 Event Selection

The reconstruction algorithms and event selection employed are refined versions of those used for previous high-mass dilepton searches [6].

3.1 Electron pair selection

To reconstruct an electron candidate, energy deposits in the ECAL are first combined into clusters of deposits under the assumption that each cluster represents a single particle. Due to bremsstrahlung emission, the original energy of the electron may be carried by many particles by the time the electron impacts the ECAL, therefore clusters are combined in a way consistent with bremsstrahlung emission to produce a single "supercluster" which represents the electron. These superclusters are used to seed tracking algorithms and if a resulting track is found, it is associated with the supercluster to form an electron candidate. The electron candidate energy is given by the energy of the associated cluster, which is adjusted through calibration and regression methods [10, 11].

Candidate electron pair events are required to have, at the HLT stage, two electron candidates with $E_T > 33$ GeV, where the transverse energy is defined as $E_{\mathrm{T}} = E \sin\theta$. To suppress hadrons misidentified as electrons, the energy deposited in the HCAL in a cone of radius $\Delta R = \sqrt{(\Delta\eta)^2 + (\Delta\phi)^2} = 0.14$ around electron candidate must be less than 15 (10)% of the ECAL cluster energy for candidates in the ECAL barrel (ECAL endcaps). Additionally, the shape of the energy deposits in the ECAL must be consistent with that of a single electron. To reduce the impact of any hypothetical L1 inefficiency at high p_{T}, for $E_T > 40$ GeV, only one of the electron candidates is required to pass the L1 trigger selection, where the L1 object can be consistent with an electron, a photon or a jet.

The event offline reconstruction follows the trigger selection. The electron candidates are required to have $E_T > 35$ GeV and satisfy $|\eta_C| < 1.4442$ (ECAL barrel region) or $1.566 < |\eta_C| < 2.5$ (ECAL endcap region) where η_C is the pseudorapidity of the cluster with respect to the nominal centre of the CMS detector. At least one of the electron candidates must be in the barrel region.

The electron candidates are also required to pass the dedicated HEEP (high energy electron pairs) selection [12], which is the same as the one used for 2015 data analysis. This ID requires electrons to be isolated in the calorimeter. The isolation requirements are that the p_{T} sum of tracks within a cone of radius $\Delta R = 0.3$ around the candidate direction to be less than 5 GeV, and the E_{T} sum of energy deposits within this same cone, with a small η-dependent offset [11], to be less than 3% of the candidate's E_{T} value.

The selected electrons are combined to form dielectron candidates. If more than one dielectron candidate is found in the event, only the two with the the two highest-p_{T} electrons is retained. Selected electron candidate pairs are not required to have opposite charge as the charge misidentification rate is large for TeV electrons.

3.2 Muon pair selection

To reconstruct a muon candidate, hits from the inner tracker and the muon system are first fitted separately to have inner tracker and standalone muon tracks and then combined in a global muon track hypothesis.

Candidate muon pair events are required to have at least one muon with track segments reconstructed in the muon detectors and with transverse momentum p_{T} above 16 GeV at L1, and

at least one muon with $p_T > 50$ GeV and $|\eta| < 2.4$ at the HLT. In order to extract the normalization factor in the control region around the Z peak ($60 < m_{\ell\ell} < 120$ GeV), a prescaled HLT trigger with a p_{T} threshold of 27 GeV is used without changing other L1 requirements.

Dedicated algorithms [13], developed for the high-p_{T} (> 200 GeV) muon offline reconstruction, are used to take account of effects of radiative processes of the high-energy muon interactions with the detector material. The muon candidates are required to have $p_T > 53$ GeV and be within the sensitive region of $|\eta| < 2.4$.

The muon candidates are also required to pass a dedicated high-momentum muon identification selection [11], which is the same as the one used for 2015 data analysis. Finally, isolated muon candidates are selected by requiring the p_{T} sum of tracks within a cone of radius $\Delta R = 0.3$ around the candidate direction to be less than 10% of the p_{T} of the candidate. The sums exclude the lepton candidate under consideration.

The selected opposite-charge muons are combined to form dimuon candidates. To ensure that the two muons originate from the same vertex a fit is performed to a common vertex. This vertex fit is required to have $\chi^2/\mathrm{dof} < 20$. To suppress background from cosmic ray muons that pass near the interaction point, the three-dimensional angle between the two track momentum vectors is required to be less than $\pi - 0.02$. In case several dimuon pairs are found in an event, only the one with the the two highest-p_{T} muons is retained.

3.3 Selection efficiencies

Single lepton trigger efficiencies are measured from data using high-p_{T} or off-shell Z bosons as a function of p_{T} and η and simulated events are weighted to account for such efficiencies. Trigger efficiency is then parametrized as a function of the invariant mass of the dilepton pair using Drell–Yan simulated events. For electrons with $E_{\mathrm{T}} > 45$ GeV, the trigger efficiency of an electron pair is 98% for events with both electrons in the ECAL barrel, and 99% for events with one electron in the ECAL barrel and the other in an ECAL endcap, and is consistent with being independent of E_{T}. The trigger efficiency of a muon pair is about 99% for events with both muons with $|\eta| < 1.2$, and 97% for events with one muon having $|\eta| < 1.2$ and the other with $\eta > 1.2$. These values are consistent with being independent of p_{T}. For events with at least one muon in the region $\eta < -1.2$, the trigger efficiency of a muon pair is about 97%.

The event reconstruction and selection efficiency, excluding the trigger request, is measured from simulated Drell–Yan events. Corrections are applied to match the behavior observed in data. The efficiency to reconstruct and select a 1 TeV electron pair within the detector acceptance is 69 ± 8% and 66 ± 10% for barrel-barrel and barrel-endcap electron pairs, respectively. The efficiency to reconstruct and select a 1 TeV muon pair within the detector acceptance is $90^{+0.5}_{-9}$% and is consistent with being independent of the pseudorapidity. The uncertainties quoted here include systematic effects.

4 Standard Model Backgrounds

The dominant and irreducible SM background to a Z′ decaying to an electron or muon pair arises from Drell–Yan $\mathrm{Z}/\gamma^* \rightarrow \mathrm{e}^+\mathrm{e}^-/\mu^+\mu^-$ process. In addition to the Drell–Yan process, lepton pairs can be produced in photon-induced (PI) process $\gamma\gamma \rightarrow \ell^+\ell^-$ from photons radiated by the incoming protons. Additional sources of background are processes which produce real prompt leptons where the two prompt leptons are from different particles, such as top quark-antiquark ($\mathrm{t\bar{t}}$), single top quark (tW), diboson (WW, WZ, and ZZ), and Drell–Yan $\tau^+\tau^-$ production, although the relative contributions of these four event types diminishes with in-

creasing dilepton mass. Multijet, W+jets and γ+jets processes also contribute, mainly in the electron channel, due to non-prompt and misidentified leptons.

The irreducible $Z/\gamma^* \to e^+e^-/\mu^+\mu^-$ background and real prompt leptons backgrounds such as $t\bar{t}$, tW, dibosons, and Drell–Yan $\tau^+\tau^-$ processes are estimated using Monte Carlo (MC) simulated events. Drell–Yan, $t\bar{t}$, tW, and WW production are simulated with the POWHEG v2 [14–19] next-to-leading order (NLO) event generator, with parton showering and hadronization described by the PYTHIA 8.2 [20] program. The Drell–Yan NLO cross sections are corrected by a mass dependent k-factor to take into account missing higher orders like QCD effects at next-to-next-to-leading order (NNLO) and electroweak effects at NLO in addition to pure QED effects. These corrections, estimated with the FEWZ 3.1 program [21] using the PDF4LHC15_nnlo_100 PDF, have a small impact on the final results.

Inclusive diboson processes are simulated at leading order (LO) with the PYTHIA program, Drell–Yan $\tau^+\tau^-$ and W+jets production at LO with the MADGRAPH 5 [22] program. The NNPDF2.3LO [23] parton distribution functions (PDFs) are used for the simulated inclusive diboson samples and the NNPDF3.0NLO [24] PDFs for the samples generated at NLO. The PDFs are evaluated using the LHAPDF library [25–27]. MRST2004qed [28] PDFs of protons including the photon contribution are used to estimate the PI background. The detector response is simulated with the GEANT4 [29] package.

The prediction from the MC simulation is validated using eμ events since the $t\bar{t}$, tW, diboson, and Drell–Yan $\tau^+\tau^-$ events all yield eμ final states that are intrinsically just as likely as the sum of ee and $\mu\mu$ final states.

For purposes of illustration in plots, all the backgrounds estimated from simulations are normalized to the data in the region of the Z boson peak (60–120 GeV).

The background arising from nonprompt and misidentified leptons occurs when one or more of the leptons is incorrectly identified as a prompt lepton. In the dimuon channel the multijet background is negligible for masses above 500 GeV. In the electron channel this background contributes less than 3% for masses above 500 GeV and is measured from data using the method described in [6].

The background from lepton pairs produced in gamma-gamma collisions from photons radiated by the incoming protons has been studied considering PDFs of the protons including the photon contribution [30]. The relative contribution of PI lepton pairs production increases with the mass, but the potential effect of this process on the derived limits is negligible.

5 Analysis strategy and results

The analysis is performed in two different categories for the electron channel, namely ECAL barrel – ECAL barrel and ECAL barrel – ECAL endcap. This separation is motivated by the different background contributions and energy resolution in each category. A similar approach is followed by the muon channel to isolate detector alignment and calibration effects in the endcap region, while have a category with the better resolution and calibration that provides higher sensitivity to new physics. Three categories are defined on this purpose considering events with: two muons in the barrel region ($|\eta| < 1.2$); at least one muon in the negative endcap ($\eta < -1.2$); one muon in the barrel region and one muon in the positive endcap ($\eta > 1.2$). This separation allows the assignment of separate uncertainties to each category.

The observed invariant mass spectra together with the predicted SM backgrounds are shown

in Figure 1 for both dielectron and dimuon events. No evidence for a significant deviation from the SM expectations is observed.

Using a Bayesian approach with an unbinned extended likelihood function, limits are derived for the production of a narrow spin-1 resonance. The likelihood function is based on probability density functions (pdf) describing the invariant mass spectra as a sum of signal and background pdfs.

The signal pdf is modeled as the convolution of a nonrelativistic Breit-Wigner with a Gaussian that accounts for the detector resolution effects. This analysis is designed for narrow resonances having a small BW intrinsic width (Γ) compared to the detector resolution. For such narrow widths, variations in Γ have typically little effect on the derived limits. The intrinsic widths of the Z'_{SSM} and Z'_{ψ} resonances are 3% and 0.6%, respectively. The resolutions are predicted by MC as a function of the generated dilepton mass and are adjusted using Z boson and cosmic ray data events. The resolution for dielectron (dimuon) pairs with a mass of 2 TeV is 1% (5.5%) for barrel-barrel pairs, 1.5% (8.5%) for barrel-endcap pairs.

The functional form of the background pdf is defined by considering the complete background set described in Section 4. For each channel, the background shape parameters of the pdfs are obtained by fitting the background distribution between 200 and 5500 GeV.

The limits are set on the parameter R_σ, which is the ratio of the cross section for dilepton production through a Z′ boson to the cross section for dilepton production through a Z or γ^* boson, measured in a mass window of 60 to 120 GeV. By performing a measurement relative to the Z boson cross section, the dependence on the integrated luminosity is removed and the impact of many experimental and theoretical systematic uncertainties is reduced.

The signal yield is given by the Poisson mean $\mu_S = R_\sigma \mu_Z R_\epsilon$, where the R_ϵ is the ratio of the selection efficiency times detector acceptance for the Z′ decay relative to the Z boson decay, and μ_Z is the Poisson mean of the number of $Z \to \ell\ell$ events, estimated by counting the number of dilepton pairs around the Z mass. The quantities μ_Z and R_ϵ are obtained separately for the dimuon and dielectron channels.

The limit-setting procedure used is nearly identical to that described in Ref. [6]. A uniform prior pdf for positive values of the signal cross section is assumed; this choice results in good frequentist coverage. Log-normal prior pdfs are assumed for the nuisance parameters representing systematic uncertainties. The acceptances are derived from simulation. The limits are sensitive to the number of signal events relative to the number of background events, and to some extent to the signal widths. To obtain the limit for a dilepton mass point, the amplitude of the background shape function is constrained using data within a mass window ± 6 times the mass resolution about the mass point. If fewer than 100 events in the 13 TeV data lie within this window, the window is symmetrically expanded until this number is reached. This procedure sets the level of the statistical uncertainty in the local background amplitude, chosen to dominate expected systematic uncertainties in the background shape at high mass. The observed limits are robust and do not significantly change for reasonable variations in the limit-setting procedure, such as modifications of the mass intervals used in the fit or changes in the assumed background shape.

The limits obtained are only valid for narrow resonances with widths of the order of a few percent of the resonance mass; correspond to on-shell cross sections and do not include model-dependent interference effects or enhancements at low mass values related to the PDFs. Within these constraints, the limits are, to a good approximation, model independent for a given spin-1 boson and production mechanism. The cross sections obtained from MC event generators

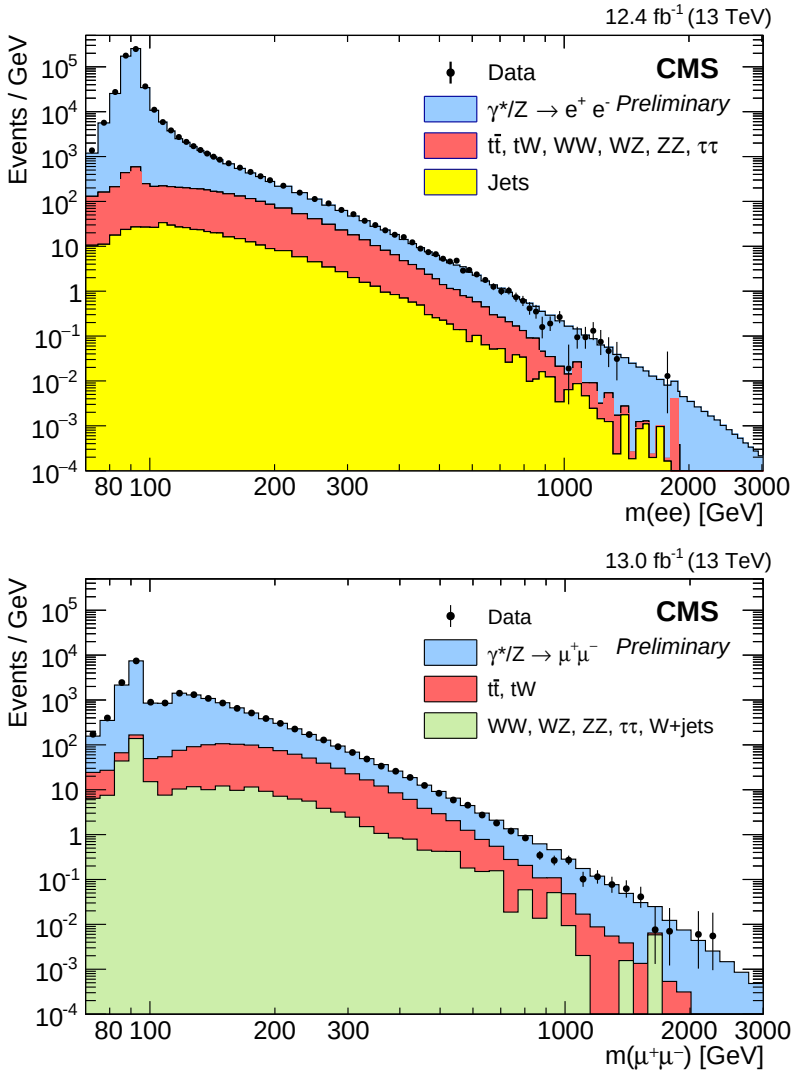

Figure 1: The invariant mass spectrum of (top) ee and (bottom) $\mu^+\mu^-$ events. The points with error bars represent the data. The histograms represent the expectations from SM processes: Z/γ^*, $t\bar{t}$ and other sources of prompt leptons (tW, diboson production, $Z \to \tau\tau$), and the multijet backgrounds. Multijet backgrounds contain at least one jet that has been misreconstructed as an electron. The MC simulated backgrounds are normalised to the data in the region of $60 < m_{\ell\ell} < 120$ GeV, with the muon channel using a prescaled lower threshold trigger for this purpose.

such as PYTHIA must be corrected as they include off-shell effects. A reasonable approximation of the on-shell cross section calculation is obtained by applying a $\pm 5\%$ $\sqrt{s}$ cut on the mass window, following the prescription in Ref [31].

The uncertainty on the signal efficiency is: 8% (10%) for the dielectron barrel-barrel (barrel-endcap) channel; $^{+1}_{-3}$% for the dimuon barrel-barrel channel; $^{+1}_{-4}$% for the dimuon positive endcap channel. A mass-dependent uncertainty is set for the dimuon negative endcap channel that vary from $^{+1}_{-4}$% at 500 GeV to -30% at 2 TeV. A mass-dependent asymmetric uncertainty ranging from -0.2% at 500 GeV to -10% (-3%) at 3 TeV is added in quadrature to this to account for the trigger efficiency uncertainty in the muon negative (positive) endcap channel. An asymmetric trigger efficiency uncertainty of -1% is set in the muon barrel-barrel channel, constant with the mass. A relative mass scale calibration uncertainty of 1% is considered when the different channels are combined. In the dimuon analysis potential misalignments in the muon chambers and track quality degradation result in uncertainties of +20% in the mass resolution.

The uncertainty in the background shape is, as noted above, dominated by the statistical uncertainty in the background amplitude estimate. In addition to the efficiency and resolution contribution, the sources of uncertainty on the background shape arise from uncertainties in the PDFs (assessed using the PDF4LHC prescriptions [32] and varying up to 10% at 5 TeV), and in the NNLO corrections to the cross sections. Photon-induced contributions are studied using the MRST2004QED and NNPDF PDFs and are found to have a negligible effect in the derived limits. The jet background in the electron analysis is a small fraction of the total background; therefore, although the uncertainty in this background is large (50%), its impact on the limit determination is negligible. Varying the numbers of background events within their total uncertainties is found to have a negligible impact on the derived limits.

The 95% CL upper limits on R_σ together with the 68% and 95% expected bands are shown in Figure 2 for both the dielectron and dimuon channels and in Figure 3 for the combination of the two channels. The resonance width is taken to be 0.6% of the assumed mass value.

The 95% CL lower limits on the masses of the Z'_{SSM} and Z'_ψ bosons are presented in Table 1, along with the expected results. The limits exclude a Z'_{SSM} with a mass less than 4.0 TeV and Z'_ψ with a mass less than 3.5 TeV. This surpasses the current best available limits of 3.36 TeV and 2.74 TeV, respectively [5, 6].

Table 1: The observed and expected 95% CL lower limits on the masses of spin-1 Z'_{SSM} and Z'_ψ bosons. The limits are rounded to the nearest 50 GeV.

Channel	Z'_{SSM}		Z'_ψ	
	Obs. (TeV)	Exp. (TeV)	Obs. (TeV)	Exp. (TeV)
ee	3.65	3.65	3.10	3.10
$\mu^+\mu^-$	3.75	3.75	3.20	3.20
ee + $\mu^+\mu^-$	4.0	4.0	3.50	3.50

6 Conclusion

A search for new narrow neutral spin-1 resonances decaying to an ee or $\mu^+\mu^-$ final state has been performed using 2016 proton-proton collision data collected at $\sqrt{s} = 13$ TeV. The data correspond to an integrated luminosity of 12.4 (13.0) fb^{-1} for the dielectron (dimuon) sample. The observations are consistent with the expectations of the standard model. Upper limits at 95% CL are set on the cross section times branching fraction for new boson production relative

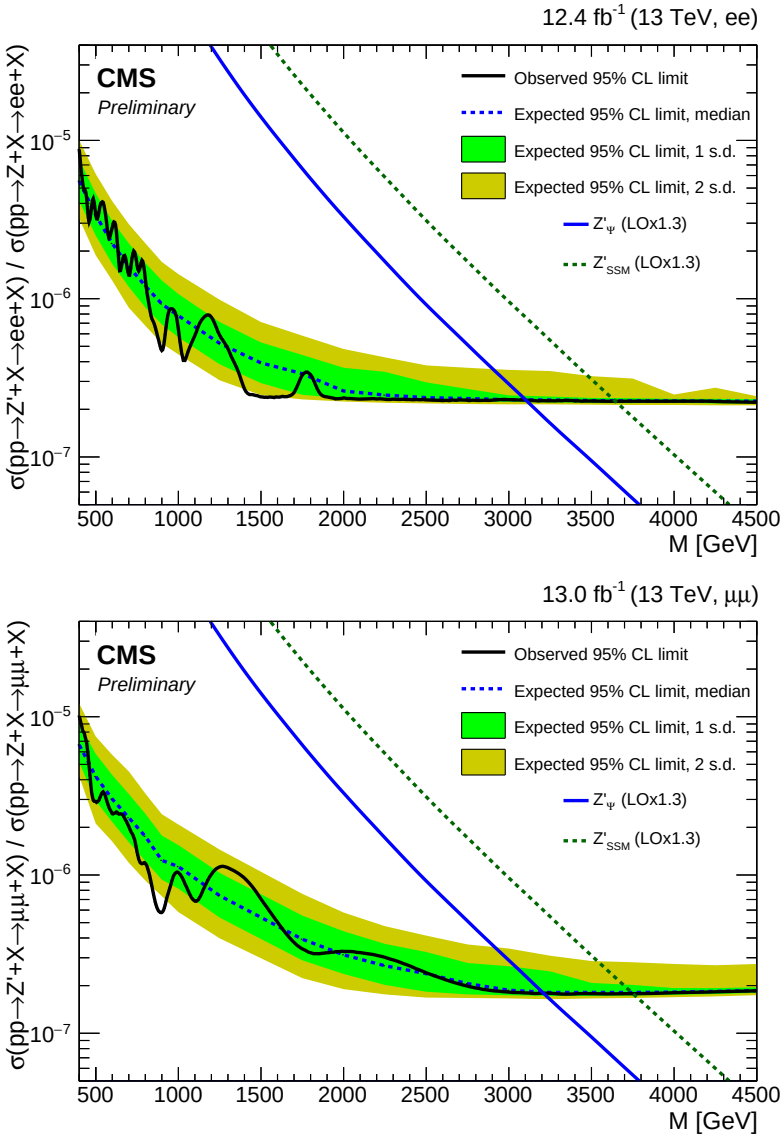

Figure 2: The 95% CL upper limits on the production cross section times branching fraction for a spin-1 resonance with a width equal to 0.6% of the resonance mass, relative to the production cross section times branching fraction for a Z boson, for the (top) dielectron and (bottom) dimuon channel. The shaded bands correspond to the 68 and 95% quantiles for the expected limits. Theoretical predictions for the spin-1 Z'_{SSM} and Z'_{ψ} resonances are shown for comparison.

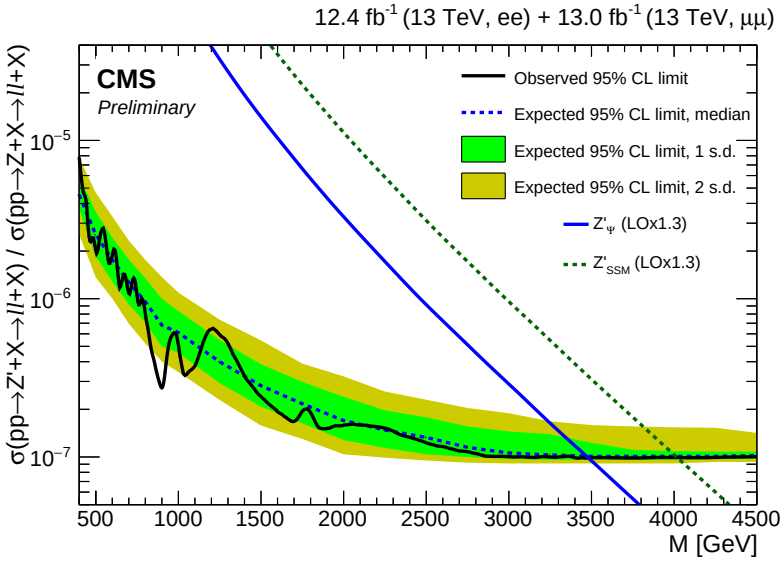

Figure 3: The 95% CL upper limits on the production cross section times branching fraction for a spin-1 resonance with a width equal to 0.6% of the resonance mass, relative to the production cross section times branching fraction for a Z boson, for the combined dielectron and dimuon channels.

to standard model Z boson production. For the Z'_{SSM} and Z'_{ψ} bosons, we obtain lower mass limits of 4.0 TeV and 3.5 TeV, respectively. These results extend the mass limits from previous searches.

References

[1] J. Ellis, "Outstanding questions: physics beyond the Standard Model", *Phil. Trans. R. Soc. A* **370** (2012) 818, doi:10.1098/rsta.2011.0452.

[2] G. Altarelli, B. Mele, and M. Ruiz-Altaba, "Searching for new heavy vector bosons in $p\overline{p}$ colliders", *Z. Phys. C* **45** (1989) 109, doi:10.1007/BF01556677.

[3] A. Leike, "The phenomenology of extra neutral gauge bosons", *Phys. Rept.* **317** (1999) 143, doi:10.1016/S0370-1573(98)00133-1, arXiv:hep-ph/9805494.

[4] J. L. Hewett and T. G. Rizzo, "Low-energy phenomenology of superstring-inspired E_6 models", *Phys. Rept.* **183** (1989) 193, doi:10.1016/0370-1573(89)90071-9.

[5] ATLAS Collaboration, "Search for new phenomena in the dilepton final state using proton-proton collisions at $\sqrt{s}$ = 13 TeV with the ATLAS detector", (2016). arXiv:1607.03669.

[6] CMS Collaboration, "Search for a Narrow Resonance Produced in 13 TeV pp Collisions Decaying to Electron Pair or Muon Pair Final States", CMS Physics Analysis Summary CMS-PAS-EXO-15-005, 2015.

[7] CMS Collaboration, "The CMS experiment at the CERN LHC", *JINST* **3** (2008) S08004, doi:10.1088/1748-0221/3/08/S08004.

[8] CMS Collaboration, "The TriDAS Project Technical Design Report, volume I: The trigger systems", CMS TDR CERN/LHCC 2000-038, CERN, 2000.

[9] CMS Collaboration, "The TriDAS Project Technical Design Report, volume II: Data acquisition and high-level trigger", CMS TDR CERN/LHCC 2002-026, CERN, 2002.

[10] M. Cacciari and G. P. Salam, "Pileup subtraction using jet areas", *Phys. Lett. B* **659** (2008) 119, doi:10.1016/j.physletb.2007.09.077, arXiv:0707.1378.

[11] CMS Collaboration, "Search for physics beyond the standard model in dilepton mass spectra in proton-proton collisions at $\sqrt{s} = 8$ TeV", *JHEP* **04** (2015) 025, doi:10.1007/JHEP04(2015)025, arXiv:1412.6302.

[12] CMS Collaboration, "Performance of Electron Reconstruction and Selection with the CMS Detector in Proton-Proton Collisions at vs = 8 TeV", *JINST* **10** (2015), no. 06, P06005, doi:10.1088/1748-0221/10/06/P06005, arXiv:1502.02701.

[13] CMS Collaboration, "Performance of CMS muon reconstruction in pp collision events at $\sqrt{s} = 7$ TeV", *JINST* **7** (2012) P10002, doi:10.1088/1748-0221/7/10/P10002, arXiv:1206.4071.

[14] P. Nason, "A New method for combining NLO QCD with shower Monte Carlo algorithms", *JHEP* **11** (2004) 040, doi:10.1088/1126-6708/2004/11/040, arXiv:hep-ph/0409146.

[15] S. Frixione, P. Nason, and C. Oleari, "Matching NLO QCD computations with Parton Shower simulations: the POWHEG method", *JHEP* **11** (2007) 070, doi:10.1088/1126-6708/2007/11/070, arXiv:0709.2092.

[16] S. Alioli, P. Nason, C. Oleari, and E. Re, "A general framework for implementing NLO calculations in shower Monte Carlo programs: the POWHEG BOX", *JHEP* **06** (2010) 043, doi:10.1007/JHEP06(2010)043, arXiv:1002.2581.

[17] S. Alioli, P. Nason, C. Oleari, and E. Re, "NLO vector-boson production matched with shower in POWHEG", *JHEP* **07** (2008) 060, doi:10.1088/1126-6708/2008/07/060, arXiv:0805.4802.

[18] S. Frixione, P. Nason, and G. Ridolfi, "A Positive-weight next-to-leading-order Monte Carlo for heavy flavour hadroproduction", *JHEP* **09** (2007) 126, doi:10.1088/1126-6708/2007/09/126, arXiv:0707.3088.

[19] E. Re, "Single-top Wt-channel production matched with parton showers using the POWHEG method", *Eur. Phys. J. C* **71** (2011) 1547, doi:10.1140/epjc/s10052-011-1547-z, arXiv:1009.2450.

[20] T. Sjöstrand et al., "An Introduction to PYTHIA 8.2", *Comput. Phys. Commun.* **191** (2015) 159, doi:10.1016/j.cpc.2015.01.024, arXiv:1410.3012.

[21] Y. Li and F. Petriello, "Combining QCD and electroweak corrections to dilepton production in FEWZ", *Phys. Rev. D* **86** (2012) 094034, doi:10.1103/PhysRevD.86.094034, arXiv:1208.5967.

[22] J. Alwall et al., "The automated computation of tree-level and next-to-leading order differential cross sections and their matching to parton shower simulations", *JHEP* **07** (2014) 079, doi:10.1007/JHEP07(2014)079, arXiv:1405.0301.

[23] R. D. Ball et al., "Parton distributions with LHC data", *Nucl. Phys. B* **867** (2013) 244–289, doi:10.1016/j.nuclphysb.2012.10.003, arXiv:1207.1303.

[24] NNPDF Collaboration, "Parton distributions for the LHC Run II", *JHEP* **04** (2015) 040, doi:10.1007/JHEP04(2015)040, arXiv:1410.8849.

[25] M. R. Whalley, D. Bourilkov, and R. C. Group, "The Les Houches accord PDFs (LHAPDF) and LHAGLUE", in *HERA and the LHC: A Workshop on the implications of HERA for LHC physics. Proceedings, Part B*. 2005. arXiv:hep-ph/0508110.

[26] D. Bourilkov, R. C. Group, and M. R. Whalley, "LHAPDF: PDF use from the Tevatron to the LHC", arXiv:hep-ph/0605240.

[27] A. Buckley et al., "LHAPDF6: parton density access in the LHC precision era", *Eur. Phys. J. C* **75** (2015), no. 3, 132, doi:10.1140/epjc/s10052-015-3318-8, arXiv:1412.7420.

[28] A. D. Martin, R. G. Roberts, W. J. Stirling, and R. S. Thorne, "Parton distributions incorporating QED contributions", *Eur. Phys. J. C* **39** (2005) 155–161, doi:10.1140/epjc/s2004-02088-7, arXiv:hep-ph/0411040.

[29] GEANT4 Collaboration, "GEANT4—a simulation toolkit", *Nucl. Instrum. Meth. A* **506** (2003) 250, doi:10.1016/S0168-9002(03)01368-8.

[30] D. Bourilkov, "Photon-induced Background for Dilepton Searches and Measurements in pp Collisions at 13 TeV", (2016). arXiv:1606.00523.

[31] E. Accomando et al., "Z' at the LHC: Interference and Finite Width Effects in Drell-Yan", *JHEP* **10** (2013) 153, doi:10.1007/JHEP10(2013)153, arXiv:1304.6700.

[32] J. Butterworth et al., "PDF4LHC recommendations for LHC Run II", *J. Phys.* **G43** (2016) 023001, doi:10.1088/0954-3899/43/2/023001, arXiv:1510.03865.